Metrol. Meas. Syst., Vol. XX (2013), No. 3, pp. 465–478.

PAN POLSKA AKADEMIA NAUK

METROLOGY AND MEASUREMENT SYSTEMS

Index 330930, ISSN 0860-8229

www.metrology.pg.gda.pl

M&MS

A SMART AND DISTRIBUTED MEASUREMENT SYSTEM TO ACQUIRE AND ANALYZE MECHANICAL MOTION PARAMETERS

J.M. Dias Pereira[1, 2)], Vítor Viegas[1, 2)], Octavian Postolache[3,4)], Pedro Silva Girão[2)]

1) Instituto Politécnico de Setúbal, ESTSetúbal/LabIM, , 2910-761 Setúbal, Portugal, (✉ dias.pereira@estsetubal.ips.pt, +351 265 790000)
2) Instituto de Telecomunicações DEEC/IST/UTL, Av. Rovisco Pais, 1, 1049-001 Lisbon, Portugal
3) Instituto de Telecomunicações/IT-IUL, Av. das Forças Armadas, 1649-026 Lisbon, Portugal
4) Instituto Universitário de Lisboa (ISCTE-IUL), Av. das Forças Armadas, 1649-026 Lisbon, Portugal

Abstract

This paper presents a low-cost and smart measurement system to acquire and analyze mechanical motion parameters. The measurement system integrates several measuring nodes that include one or more triaxial accelerometers, a temperature sensor, a data acquisition unit and a wireless communication unit. Particular attention was dedicated to measurement system accuracy and compensation of measurement errors caused by power supply voltage variations, by temperature variations and by accelerometers' misalignments. Mathematical relationships for error compensation were derived and software routines for measurement system configuration, data acquisition, data processing, and self-testing purposes were developed. The paper includes several simulation and experimental results obtained from an assembled prototype based on a crank-piston mechanism.

Keywords: measurement system, kinematic variables measurements, accelerometers, error compensation, accuracy.

1. Introduction

Amplitude, phase and frequency measurements of kinematic variables, namely position, velocity and acceleration, are essential to a huge number of applications that include condition monitoring of machinery devices. This paper presents a low-cost measurement system to acquire and analyze mechanical motion parameters. The proposed measurement system includes several measuring nodes (MNs) with sensing, data conditioning, analog to digital conversion and data transmission capabilities. It is important to underline that wireless communication capability of the MN is essential in this type of application since data acquisition from moving devices does not allow usually the use of wired connections. Moreover, it is important to refer that the distributed topology of the measurement system allows simultaneous measurements of kinematic variables, namely position, velocity and acceleration, among others, at different measurement points, being possible to establish cross-correlations between measurement data acquired in different MNs [1-4]. Measurement system fault detection routines can be easily implemented by using the measurement data of each MN, considering, for example, the expected measuring range of each variable or the cross-correlation that is expected between different measuring quantities [5-7]. Obviously, this advantage can only be achieved if the theoretical model of the system is known or if the mechanical device under test had been previously characterized. Concerning monitoring purposes, it must be underlined that abnormal variation of kinematic parameters indicates potential failures of the mechanical devices under analysis [8-10]. Thus, monitoring of mechanical devices, particularly the ones that are submitted to hard working conditions, is

Article history: received on Nov. 12, 2012; accepted on Jun. 06, 2013; available online on Sep. 15, 2013; DOI: 10.2478/mms-2013-0040.

essential to schedule predictive maintenance [11] and then to improve mechanical systems' reliability.

In order to improve measurement accuracy, several error compensation techniques are presented [12-14]. In this context, steady state measurements of the mechanical device, namely tilt measurements of mechanical elements, can be used to compensate misalignment measurement errors since it is particularly important to extract from the accelerometer signal the component that is associated with gravity acceleration [15]. Otherwise, the acceleration component that is associated with the mechanical motion will be mixed with tilt components that result from the relative positioning of the mechanical elements associated with each MN. Other errors, like the ones caused by temperature variations that can substantially affect measurement accuracy, are also compensated; otherwise, it will be impossible to distinguish mechanical motion parameter variations from the ones that are caused by temperature variations.

Regarding applications of the proposed measurement system, it can be said that it can be used in a large number of industries that employ power transmission units and components, like linear actuators, clutches and automotive timing chain drive systems used to drive camshafts in auto engines [16]. Other typical examples that can illustrate systems' applications in industrial environments occur in the synchronization that must exist between different running shafts of a computer numerical control (CNC) machinery [4], [17] or in the coordination of robots that exhibit the capability to execute movements of multiple axes [18-19]. Others types of applications are related with vibration measurements that are very important to evaluate the performance of industrial plants, namely the measurement of piping structures, motors and control valve vibrations, among others, which are essential to schedule corrective and predictive maintenance tasks based on regular or continuous monitoring results [20].

It is important to underline that there exist some commercial solutions for identical measurement purposes, however, these solutions are very expensive, proprietary and their flexibility to define new measurement configurations and data processing algorithms, suitable for specific applications, is very low [21].

This paper is organized in five sections. The present one is the introduction, section two describes the measurement system, namely its hardware and software parts, section three is dedicated to measurement error compensation, section four includes simulation and experimental results and the last section, section five, is dedicated to conclusions.

2. System description

This section includes the description of the measurement system hardware and software components, underlining their main characteristics.

2.1. Hardware

The hardware of the measurement system includes several measuring nodes (MNs) and a coordinator node (CN).

It is important to underline that the number of sensors in each MN is selected according to users' requirements and mechanical device under test (MDUT) characteristics. Fig. 1 represents a typical MN block diagram that includes two accelerometer devices and a temperature sensor. Additional sensing elements can be included in each MN according to the type and the number of quantities that must be measured. Measurement tests were performed with other sensor types, namely, vibration sensors, pressure sensors and encoders.

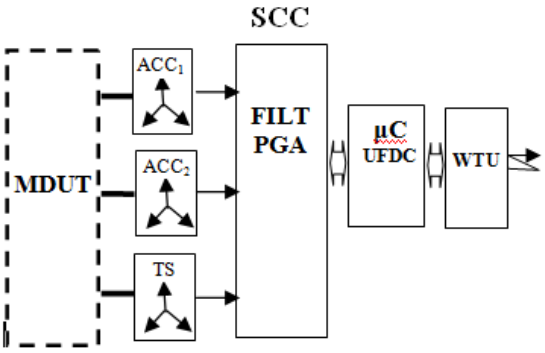

Fig. 1. Measuring node block diagram (MDUT- mechanical device under test, ACC- accelerometer, SCC- signal conditioning circuits, FILT- filter, PGA- programmable gain amplifier, µC- microcontroller, UFDC- universal frequency to digital converter, WTU- wireless transmission unit).

The signal conditioning unit includes mainly an analog filter and a programmable gain amplifier. The analog filter is a fourth order Butterworth low-pass filter with a cutoff frequency equal to 3 kHz and the programmable gain amplifier is implemented with an instrumentation amplifier whose gain is adjusted by a digital potentiometer [22]. The processing and control tasks of each MN are performed by a microcontroller whose data memory stores, in addition to measurement data, several configuration parameters including transducer electronic data sheet (TEDS) parameters [23] of the different transducers contained in each MN. Fig. 2 depicts a schematic representation of the whole measurement system for a 3 MNs topology. The wireless communication network is supported by Bluetooth-TTL transceivers used to interconnect the CN with the different MNs.

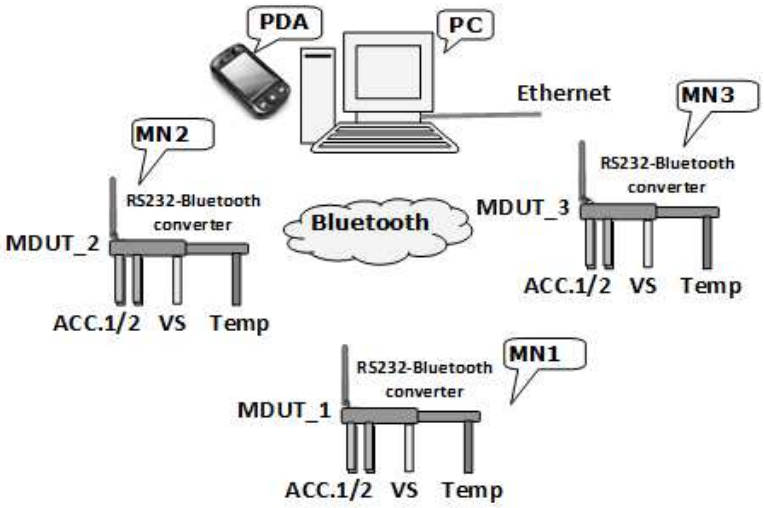

Fig. 2. Schematic representation of the whole measurement system (CN- coordinator node, MN- measuring node, MDUT- mechanical device under test, ACC- accelerometer, PC- personal computer, PDA- personal data assistant).

The calibration of the measurement system was performed with a multifunction data acquisition (DAQ) board [24].

2.1.1. Transducers

Regarding acceleration measurements, a low-cost MEMS (Micro-Electro Mechanical System) [25-26] accelerometer from Analog Devices [27] was selected to perform triaxial acceleration measurements. The main characteristics of the accelerometer include a measurement range between -3 *g* and 3 *g*, nominal sensitivity equal to 300 mV/g for a power supply voltage equal to 3 V (ratiometric dependence), a temperature drift equal to 25 mV/ ^{o}C, a temperature working range between -25 ^{o}C and 70 ^{o}C and non-linearity equal to 0.015 % of full scale amplitude (FS). A set of three external capacitors of 10 nF were used to define a 3 dB filter bandwidth of 500 Hz with a low cut-off frequency equal to 0.5 Hz for each accelerometer's measuring axis. An additional characteristic of the accelerometer that improves the reliability of the measurement system is its self-test capability. Self-testing is performed by applying a square wave voltage to each self-test (ST) input of the integrated circuit and checking the output voltage waveform and amplitude.

To compensate measurement errors caused by temperature variations, an integrated temperature sensor SMT 160-30 [28] with a temperature dependent duty cycle output signal was included in the measurement system. The main characteristics of the temperature transducer includes an accuracy better than 0.7 ^{o}C, a linearity output error lower than 0.2 ^{o}C, a resolution better than 0.005 ^{o}C and repeatability better than 0.1 ^{o}C for a temperature measurement range between -30 ^{o}C and 100 ^{o}C. The duty cycle of the output signal is linearly related to the temperature according to the following relationship:

$$DC_y = 0.320+0.00470 \cdot T \quad (1)$$

where DC_y represents the duty cycle and T represents the temperature in °C.

A UFDC [29] integrated circuit, programmed for duty cycle measurements, was used to perform the digitalization of the temperature signal.

Concerning temperature measurements, it is important to refer that whenever required, for example for large machine tools, additional temperature sensors can be included in each MN to improve temperature measurement accuracy. Moreover, if the average of temperature measurements is calculated for N_T sensors, there is a theoretical repeatability improvement of factor equal to $1/\sqrt{N_T}$. It is also important to underline that from the temperature measurements obtained in different MNs, it is possible to obtain the temperature spatial gradient, this information being particularly important to detect and prevent potential faulty conditions of the MDUT.

2.1.2 Signal conditioning and A/D conversion

The signal conditioning unit includes several commercial off-the-shelf (COTS) electronic components that perform impedance matching, signal filtering and signal amplification. A fourth order Butterworth low-pass filter is used to improve the signal-to-noise ratio of the accelerometer signal and to avoid spectral aliasing effects of vibration signals. The filter cut-off frequency can be automatically adjusted using digital potentiometers [22] but its value is by default equal 3 kHz . The programmable gain amplifier that was implemented with an instrumentation amplifier improves the measurement accuracy and resolution for low amplitude signals. Analog to digital conversion (ADC) of accelerometer signals is implemented by the internal 10 bit A/D channels of the microcontroller [30] and the output duty cycle signal provided by the temperature sensor is digitized using a universal frequency to digital converter. The microcontroller memory stores several TEDS parameters that are used to identify the measurement node and the sensor characteristics, namely their sensitivity, the calibration date and the calibration coefficients. A multifunction data acquisition board

(NI-USB 9162) was used for calibration purposes. The main characteristics of the DAQ board include a set of 4 simultaneously sampled analog inputs, a maximum sampling data rate equal to 100 kS/s, 16-bit resolution, an accuracy equal to ±0.67% of the input voltage full-scale (10 V), and an offset error equal to ±1.25% of FS amplitude. The simultaneous sampling capability of the DAQ board avoids data processing errors caused by sampling delays between the different data acquisition channels.

2.1.3 Wireless communication unit

A wireless Bluetooth-TTL transceiver module was used to implement wireless communication between the MN and the personal computer data processing unit that works as a CN [31]. The main characteristics of the transceiver device include a power supply voltage of 3 V, maximum power consumption lower than 210 mW, an RF transmitter power of +2 dBm and a typical receiver sensitivity of -80 dBm for a 0.1 % bit error rate (BER). These specifications fulfill entirely all measurement system requirements. Fig. 3 depicts the front view of the printed circuit board (PCB) and shows some components of the signal conditioning unit, the microcontroller and the wireless transceiver unit (WTU).

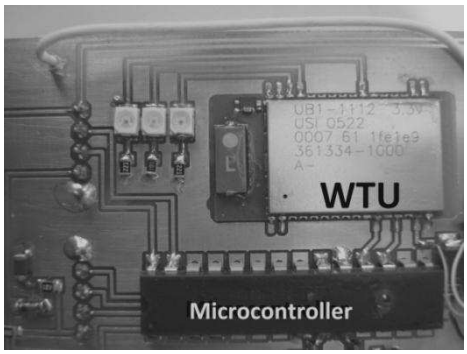

Fig. 3. Front view of the printed circuit board (PCB).

2.2. Software and data processing

The software of the measurement system includes a set of routines that performs measurement system configuration, digital signal processing, data communication control and fault detection. The parameters used to perform the digital filter configuration include the filter type, its order, and bandwidth. By default, a fourth order Butterworth low-pass filter with a cutoff frequency equal to 3 kHz is selected but second order active universal filters [32] were also tested successfully. Parameters related with the data acquisition configuration include data sampling rate, number of samples to acquire, and data acquisition channels configuration. The configuration of the UFDC includes the following parameters: measuring mode (duty cycle measurement), measurement accuracy, and resolution.

Several programs were developed to analyze measurement data according to the main characteristic of the mechanical device under analysis. Curve fitting algorithms [33] were developed to perform signal analysis, signal to noise ratio evaluation and measurement of mechanical system performance.

Fig. 4 represents the front panel of the LabVIEW [34] program that was used for accelerometer testing purposes. The upper graphs represent the triaxial acceleration signals extracted from the accelerometer under test, the lower graphs represent the rotary speed sensor (RSS) [35] signal and the power spectrum of the vibration signal. Indicators of power harmonic distortion (THD), for each accelerometer axis, are also displayed on the lower right part of the user interface panel.

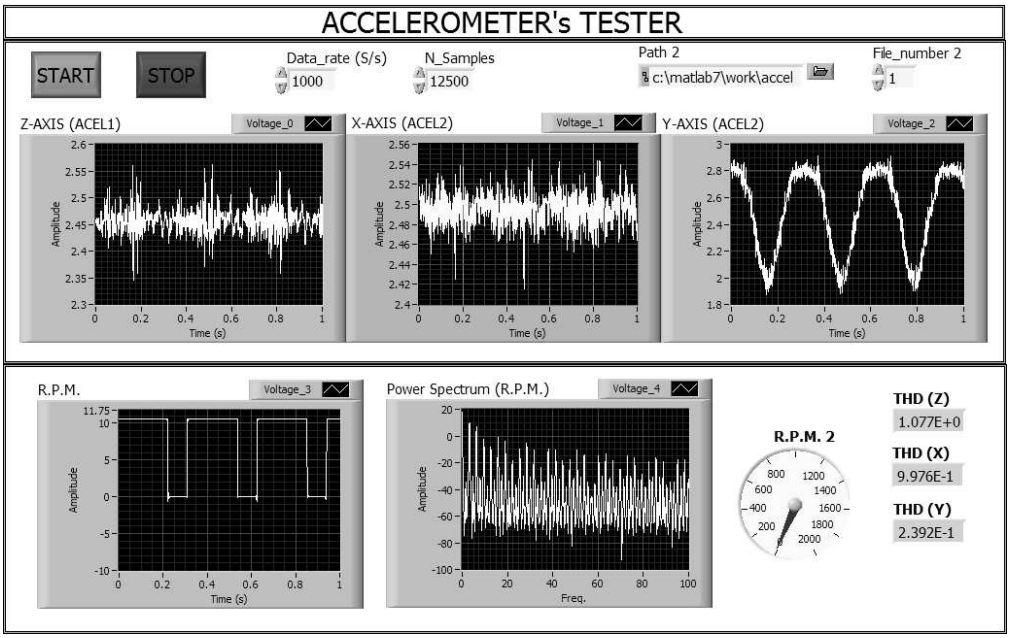

Fig. 4. Front panel of the data acquisition program.

It is important to underline that different routines were developed to perform error compensation and to improve measurement accuracy, namely, to compensate errors caused by accelerometer or mechanical system misalignments, temperature and power supply voltage variations, as well as to store measurement data records with time-stamp information. Using the database measurement records, stored over time, it is possible to display and analyze the time evolution of the measuring data and to prevent potential faulty conditions that will affect the MDUT reliability.

3. Error compensation

Besides off-line calibration of the offset and sensitivity of each accelerometer using the gravity test method [36], three on-line self-calibration routines were developed to compensate errors caused by accelerometer or mechanical system misalignments and temperature and power supply voltage variations. Higher levels of measurement accuracy can be achieved by using calibrators with much lower measurement errors.

3.1. Misalignment errors

A common source of errors in measurement systems that include multiple-axis accelerometers are related with the deviation between ideal and real measuring axes. This deviation is caused not only by inter-axis alignment errors of the accelerometer but also, and above all, by positioning alignment errors of the accelerometers over the measuring surfaces where they are mounted or by misalignments of the MDUT. To minimize the negative impact of these errors in terms of measurement system accuracy, tilt measurements can be used to compensate their effect. Considering the tri-orthogonal referential represented in Fig. 5, it is possible to compensate static errors that are caused by accelerometers' misalignments taking the direction of gravity vector as a reference.

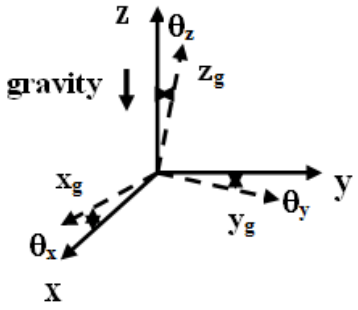

Fig. 5. Tri-orthogonal referential used to evaluate misalignment errors (θ_x, θ_y and θ_z represent the misalignment between ideal measuring axes and accelerometers' sensitive axes).

If X, Y, and Z represent the tridimensional axes directions, X_g, Y_g, and Z_g the tridimensional accelerometer sensitive axes directions, and θ_x, θ_y, and θ_z, the direction misalignment between ideal measuring axes and accelerometer sensitive axes, the matric relationship that can be used to perform error compensation is given by

$$\begin{bmatrix} a_{xc} \\ a_{yc} \\ a_{zc} \end{bmatrix} = \begin{bmatrix} \alpha_{11} & \alpha_{12} & \alpha_{13} \\ \alpha_{21} & \alpha_{22} & \alpha_{23} \\ \alpha_{31} & \alpha_{32} & \alpha_{33} \end{bmatrix} \begin{bmatrix} a_x \\ a_y \\ a_z \end{bmatrix} \tag{2}$$

where a_x, a_y, and a_z, represent the triaxial acceleration values, a_{xc}, a_{yc}, and a_{zc} represent their compensated values and α_{ij} represent the misalignment error coefficients.

Assuming there is no cross-dependence between axial alignment errors, the previous matric relationship can be simplified yielding the following set of equations

$$\begin{aligned} a_{xc} &= a_x \cdot \sec(\theta_x) \\ a_{yc} &= a_y \cdot \sec(\theta_y) \\ a_{zc} &= a_z \cdot \sec(\theta_{zx}) \end{aligned} \tag{3}$$

where sec(x) represents the trigonometric operator given by the inverse of cos(x) function.

3.2. Temperature errors

Another source of errors is related with temperature variations, particularly the change of accelerometer sensitivity with temperature. Using a linear approximation of the sensitivity variation with temperature, and assuming that the temperature dependence is the same for each accelerometer axis, the following set of equations can be used to compensate measurement errors caused by temperature variations:

$$\begin{cases} a_{xc} = a_x/[1 + \beta \cdot (T - T_0)] \\ a_{yc} = a_x/[1 + \beta \cdot (T - T_0)] \\ a_{zc} = a_x/[1 + \beta \cdot (T - T_0)] \end{cases} \tag{4}$$

where β represents temperature sensitivity and T_0 represents the reference temperature, typically equal to 25 ^oC.

To evaluate the amplitude of these errors, experimental tests were performed using a digital programming oven submitted to a temperature variation cycle between 35 ^oC and 75 ^oC. The results that were obtained showed an accelerometer output voltage variation between 2.83 V and 3.00 V for the previous temperature range. This variation can reduce substantially measurement system accuracy since it corresponds to a measurement error about 0.56 *g* for the accelerometers included in the measurement system.

3.3. Errors caused by power supply voltage variations

A large number of accelerometer parameters are ratiometric, which means that the output signal amplitude of those devices is directly proportional to the power supply voltage amplitude. Errors caused by power voltage variations can be substantially high if the power supply is not well regulated or exhibits amplitude variations over time [37]. In order to compensate these errors, one of the A/D inputs of the microcontroller is used to convert the power supply voltage amplitude and then all the accelerometers' measurements are scaled relatively to the nominal power supply voltage amplitude [38]. If the power supply voltage amplitude is not contained in the operating voltage range a faulty condition is detected and an alarm message is triggered.

4. Simulation and experimental results

Experimental tests of the measurement system were performed using a single crank-piston mechanism interconnected to an electrical motor through a belt drive system (BDS) [39]. Using this test setup a sinusoidal-like motion with adjustable values of amplitude and frequency was generated to evaluate the performance of the measurement system. It is important to underline that the experimental accuracy values that will be presented can be substantially improved since the low-cost prototype implemented using off-the-shelf components was designed for teaching purposes and not for commercial and accurate applications.

4.1. Mechanical model and simulation results

The kinematic equations of the position, velocity and linear acceleration of the crank-piston mechanism are easily obtained using the geometrical model represented in Fig. 6. In that figure, l represents the connecting rod length, r represents the crank radius and x represents the position of the piston from crank, being P the piston pin, N the crank pin and O the crank centre.

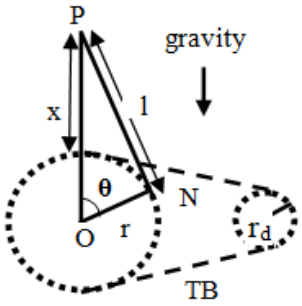

Fig. 6. Geometrical model of a crank-piston mechanism (l- rod length, r- crank radius, rd- driven pulley radius, x- position of the piston from crank, P- piston pin, N- crank pin, O- crank centre and TB- transmission belt).

The kinematic equation of the piston acceleration is given by [40],

$$a = \frac{\partial^2 x}{\partial t^2} = -r \cdot \alpha - \frac{r \cdot (\alpha^2 - \beta^2)}{(l^2 - r^2 \cdot \beta^2)^{1/2}} - \frac{r^4 \cdot \alpha^2 \cdot \beta^2}{(l^2 - r^2 \cdot \beta^2)^{3/2}} \quad (5)$$

where $\alpha=\cos(\theta)$ and $\beta=\text{sen}(\theta)$.

Assuming that the crank pin (N) has a uniform circular motion, $\theta=\omega \cdot t$, where ω represents the angular frequency, some simulations were performed to compare the experimental results

that are obtained with their theoretical expectations. Fig. 7 represents the simulation results of the piston acceleration for three different values of the crank radius length, namely: r=1 cm, r=1.5 cm and r=2 cm, using identical values of rotation speed (freq.=5 Hz) and a connecting rod length (l) equal to 4 cm. The simulation results clearly show that the profiles of the acceleration curves are strongly dependent on the geometrical parameters of the crank-piston mechanism. It is clearly visible that for a crank radius length (r) equal to zero there is no crank effect, the piston is stationary, and as the crank radius length increases the piston motion starts to be almost sinusoidal and then tends to exhibit increasing values of total harmonic distortion (THD). Then, the selected mechanical model is effective to test the measurement system since different working conditions can be easily obtained by varying the crank radius (r) or the connecting rod length.

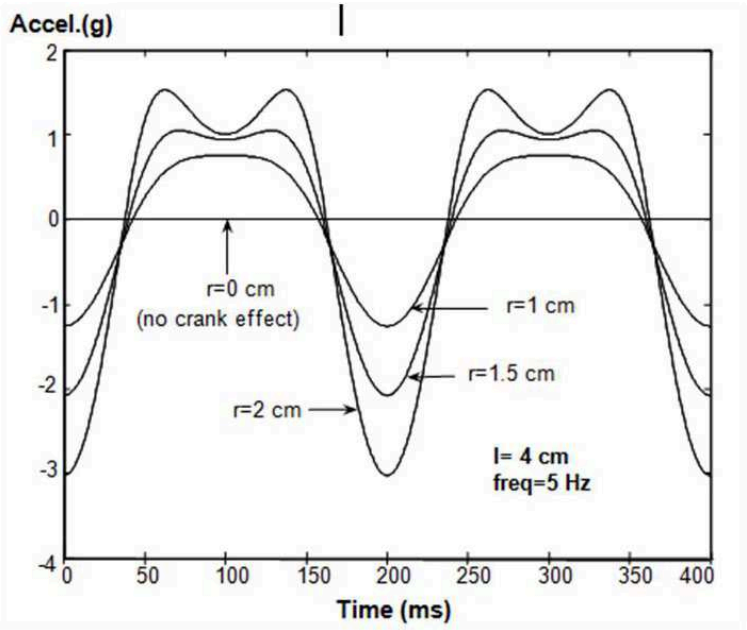

Fig. 7. Simulation results of the piston acceleration for different values of the crank radius: r=0 cm, r=1 cm, r=1.5 cm and r=2 cm.

4.2. Experimental results

Regarding experimental tests, a prototype based on a crank-piston unit of a motorbike engine actuated by an electrical engine that is controlled by a variable speed driver [41] was assembled. It is important to underline that the testing prototype was implemented using low-cost commercial off-the-shelf components. Fig. 8(a) depicts the experimental set up that was used for testing purposes and Fig. 8(b) depicts an assembly detail of the triaxial accelerometer that was placed over the piston. The measurement system contains three MNs, namely: MN1, that includes a triaxial accelerometer mounted over the piston, a temperature sensor and a rotation speed sensor; MN2, that includes a second triaxial accelerometer mounted over the crank, and MN3, that includes a third triaxial accelerometer mounted on the motor shaft.

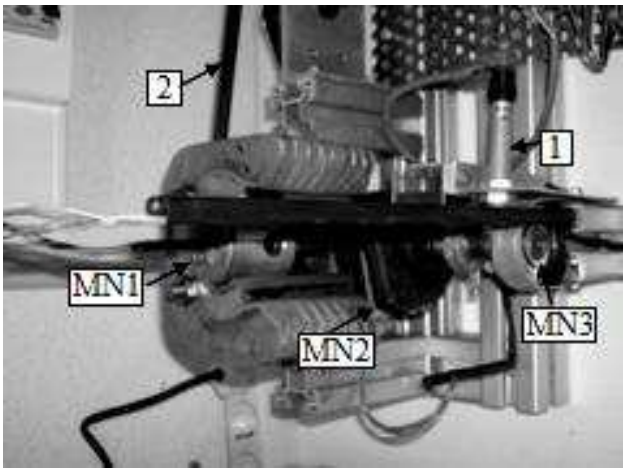

(a)

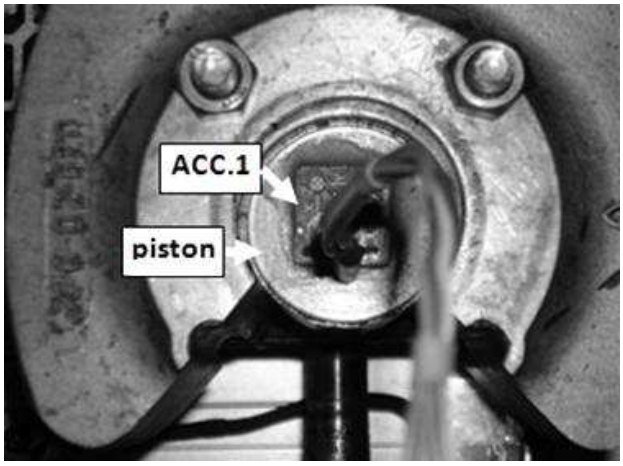

(b)

Fig. 8. (a) Experimental set up used for testing purposes (MN1- piston measuring node, MN2- crank measuring node, MN3- motor shaft measuring node, 1- rotary speed sensor, 2- transmission belt; (b) assembly detail of the triaxial accelerometer placed over the piston.

It is important to refer that the measurement variables accessed by MN1 contain redundant data that can be used for self-testing purposes. The angular speed can be obtained directly from the rotation speed sensor but it can also be obtained, indirectly, from the accelerometer. The use of data correlation operators between motion variables obtained in different MNs of the MDUT can also be used for self-testing or fault detection purposes.

Figure 9 represents the triaxial acceleration signals that were measured by the accelerometer and by the RSS that are included in MN1, for a crank rotating frequency equal to 2 Hz. It is clearly visible that “x” and “y” axis acceleration components are almost null and the “z” axial acceleration component has a peak-to-peak amplitude approximately equal to 600 mV that corresponds, according to the nominal sensitivity of the accelerometer, to a peak-to-peak acceleration amplitude almost equal to 2 g. The axial “x” and “y” acceleration components were expected to be almost null since the accelerometer is mounted over the piston plane that is orthogonal to the gravity direction. It should be emphasized that the gravity acceleration signal component, obtained from tilt measurements, was removed from the accelerometer signals in order to obtain the acceleration component that results from MDUT motion.

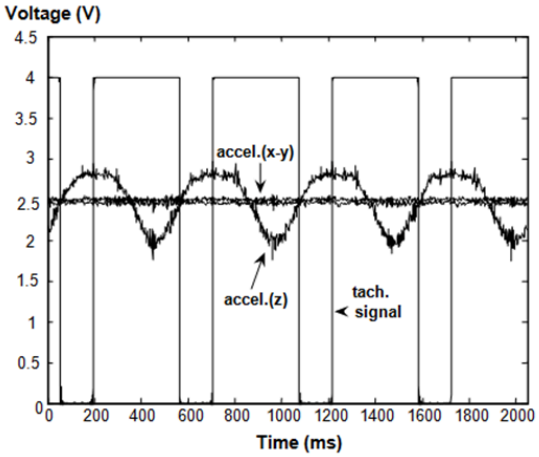

Fig. 9. Triaxial acceleration and rotary speed sensor signals captured in MN1.

A second experimental test was performed with measurement data collected from the three measuring nodes. Fig. 10 represents the measured and curve fitting data that was obtained in each MN for the following set of testing parameters: l=4 cm, r=2 cm and freq=4 Hz. The signals that are represented include the "z" axial component of the acceleration signal extracted from ACC.1 that is mounted over the piston, and the angular speed signal extracted from the RSS signal; for the MN2 the "y" axial component of the acceleration signal extracted from ACC.2 that is mounted over the crank shaft and the "y" axial component of acceleration signal extracted from ACC.3 that is mounted over the motor shaft.

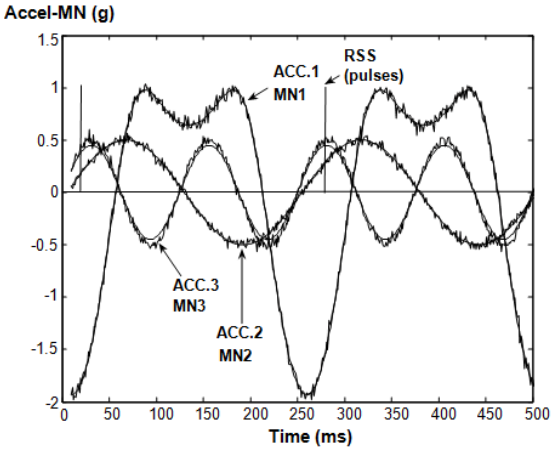

Fig. 10. Measured and curve fitting data that were obtained in the three MNs for the following set of testing parameters: l=4 cm, r=2 cm and freq=4 Hz (MN1- ACC.1_Z and RSS, MN2- ACC.2_Y and MN3- ACC.3_Y).

Fig. 10 clearly shows that there is a ratio almost equal to two between the periods of the signals extracted from ACC.2 and ACC.3, which agrees with the experimental value of the gear ratio of the transmission belt.

4.3. Signal to noise ratio

In order to evaluate the signal to noise ratio of the measurement system, an experimental test was performed with the following set of parameters: l=4 cm, r=2 cm and freq=4 Hz. Fig. 11(a) represents the measured and curve fitting data that were obtained using the analytical relationship (5), and Fig. 11(b) represents the relative error defined as the ratio, in percentage, of the difference between measured and data curve fitting values and the accelerometer full scale amplitude (*3g*). A modified version of the simplex Nelder-Mead algorithm [42] was

used to find the set of piston-crank dimensional parameters (l,r) and the rotation frequency (f) that minimizes the difference between measurement and curve fitting data.

From the experimental data that was obtained it possible to verify that there is a signal-to-noise ratio of the measurement signal almost equal to 19 dB.

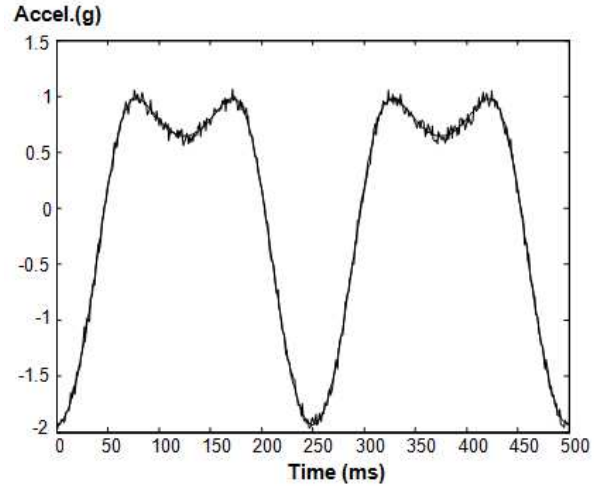

(a)

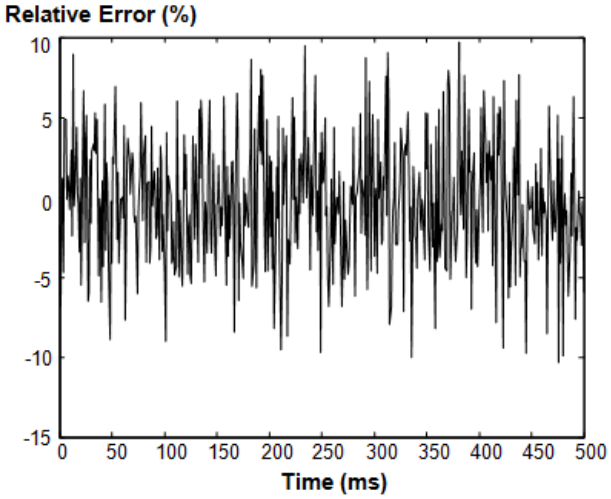

(b)

Fig. 11. (a) Measured and curve fitting data that were obtained for the following set of parameters: l=4 cm, r=2 cm and freq=4 Hz; (b) Relative error between measurement curve fitting data.

It is important to underline that dithering, noise shaping, digital filtering, and decimation techniques can be used to improve the signal-to-noise ratio and the resolution of the measurement system, obviously, at the expense of input signal bandwidth [43].

5. Conclusion

A wireless measurement system based on a set of different measuring nodes that include one or more accelerometers, a temperature sensor, a data acquisition unit and a wireless communication unit was presented. Curve fitting techniques were successfully used to evaluate the deviation between experimental data and the theoretical data derived for the kinematic equations of the MDUT. Particular attention was dedicated to the measurement system accuracy and to the compensation of the measurement errors caused by power supply voltage variations, by temperature variations, and by accelerometers' or mechanical system misalignments. Experimental tests were performed using a crank-piston mechanism and a

measurement system with three measuring nodes. The experimental results that were obtained confirmed the theoretical expectations based on the kinematic equations of the mechanical device under test. Finally, it is important to underline that the accuracy values that were obtained can be substantially improved, since the low-cost prototype that was used to perform the experimental tests was designed for teaching purposes and not for accurate measurements.

References

[1] Abuthakeer S.S., Mohanram P.V., Mohankumar G. (2011). The Effect of Spindle Vibration on Surface Roughness of Workspiece in Dry Turning Using ANN. *International Lean Thinking*, Vol. 2, Issue 2.

[2] Tobias S. et al. (2005). Influence of Surface Roughness on Friction During Metal Forming Processes. *Journal of Materials Processing Technology*. 159, 9-16.

[3] Li Y., Lin J., Wang X., Liao Y. (2011). Multiple-axis synchronization evaluation for CNC machine tool based on sensor less measurement. *In Proceedings of IEEE International Symposium on Assembly and Manufacturing (ISAM)*, Vol.1, 1-5.

[4] Albarbar A., Mekid S., Starr A., Pietruszkiewicz R. (2008). Suitability of MS Accelerometers for Condition Monitoring: An experimental study. *Sensors*, Issue (8), 784-799.

[5] Liming Wu, Junxiu L., Ji Zhang, Yuling L. (2009). *The Intelligent Reconfigurable Measuring Node. Proceedings of the International Conference on International Conference on Computational Intelligence and Security* (CIS '09), Vol. 1, 570-573.

[6] Chao Fan, Zhang De-xian, Hong-liang Fu, Yi-tao Liang (2010). Design of the Measurement Node of the Grain Quantity Monitoring System Based on the CAN-bus. *Proceedings of the International Conference on Challenges in Environmental Science and Computer Engineering (CESCE),* Vol. 1, 211-214.

[7] Peng Faya (2005). Design considerations for a distributed test system. In *Proceedings of IEEE Autotestcon*, 235-239.

[8] Aidemark J., Folkesson P., Karlsson J. (2005). A framework for node-level fault tolerance in distributed real-time systems. In *Proceedings of International Conference on Dependable Systems and Networks*, 656-665.

[9] Ananthanarayanan S.P., Szymczyk C., Goldenberg A.A. (1992). Identification of kinematic parameters of multiple closed chain robotic manipulators working in coordination. In *Proceedings of IEEE International Conference on Robotics and Automation*, Vol. 1, 358-363.

[10] Zhang Bin et al. (2011). A Probabilistic Fault Detection Approach: Application to Bearing Fault Detection. *IEEE Transactions on Industrial Electronics*, Vol. 58, Issue 5, 2011-2018.

[11] Dayly J.W., Riley W.F., McConnell (1984). *Instrumentation for Engineering Measurements*. New York, NY: John Wiley & Sons.

[12] Wanli Liu, Xinghu Q, Yonggang Y (2007). Self-Calibration and Error Compensation of Flexible Coordinate Measuring Robot. In *Proceedings of International Conference on Mechatronics and Automation*, 2489-2494.

[13] Kermorgant O., Folio D., Chaumette F. (2010). A new sensor self-calibration framework from velocity measurements. In *Proceeding of Conference on Robotics and Automation*, 1524-1529.

[14] Li X, et al (2011). An error compensation method for multi-axis machining based on the actual contour measurement. In *Proceedings of IEEE International Symposium on IEEE International Symposium on Assembly and Manufacturing*, 1-5.

[15] Alloca J.A., Stuart A. (1984). *Transducers Theory & Applications*. Reston Publishing Company, Inc., Prentice-Hall.

[16] Tsubakimoto Chain CO., Automotive Parts Products (April, 2012). *http://tsubakimoto.com.*

[17] Mahrenholtz O., Bontcheva N., Iankov R. (2005). Influence of surface roughness on friction during metal forming processes. *J. Mater. Process. Technology,* No. 159, 9-16.

[18] Quigley M., Brewer R., Soundararaj S.P., Pradeep V., Quoc Le Ng A.Y (2010). Low-cost accelerometers for robotic manipulator perception. *In Proceedings of Internation Conference on Intelligent Robots and Systems (IROS)*, Vol. 1, 6168-6174.

[19] Renk E.L., Rizzo M., Collins W., Lee F., Bernstein D.S.. Calibrating a triaxial accelerometer-magnetometer - using robotic actuation for sensor reorientation during data collection. *IEEE Control Systems,* Vol. 25 , Issue 6 , 86-95.

[20] Dias Pereira J.M., Postolache O., César M.L., Girão P.S (2012). A Smart Sensing System to Analyze Piping Vibrations in Industrial Installations. *In Proceedings of the International Conf. on Sensing Technology (ICST 2012)*, Vol. 1, 7-14.
[21] Midé Technology. Slam Stick™ Vibration Recorder (2012 Sept.). *http//:www.digikey.com/uk/en/ph/mide/slamstick.html.*
[22] Dallas Semiconductor, DS1809 Dallastat™ - 64-position digital potentiometer (2010 Sept.) *http://www.datasheets.maxim-ic.com/en/ds/DS1809.pdf.*
[23] National Instruments. An Overview of IEEE 1451.4 Transducer Electronic Data Sheets (2010 Sept.). *http://www.standards.ieee.org/develop/regauth/tut/teds.pdf.*
[24] National Instruments. Data Acquisition Board- 9215 (2010 Sept.). *http://www.sine.ni.com/nips/cds/view/p/lang/en/nid/208793.*
[25] Abdelhamid M.K. (2003). Towards Smarter Measurement Systems. In *Proceedings of Conference - IMAC-XXI: Conference & Exposition on Structural Dynamics*. *https://www.sem.org/Proceedings/ ConfPapersPaperID=25721.*
[26] Yurish S.Y., Gomes M.T. (2004). *Smart Sensors and MEMS. II Mathematics, Physics and Chemistry*, Vol. 181, NATO Sciences Series, Kluwer Academic Publishers.
[27] Analog Devices, iMEMS Accelerometer ADXL330 (2010 Sept.). *http://www.datasheetarchive.com/ADXL330KCPZ-datasheet.html*.
[28] Smartec, SMT 160-30 Temperature Sensor (2010 Sept.). http://www.smartec-sensors.com.
[29] International Frequency Sensor Association, Universal Frequency-to-Digital Converter (Sept. 2010). *http:// www.sensorsportal.com.*
[30] Microchip Technology Inc., PIC16F87X Microcontrolle (2010 Sept.). *http://www.microchip.com.*
[31] MDFLY Electronics, Wireless Bluetooth TTL Transceiver Module (Sept. 2010). *http:// www.mdfly.com*
[32] Texas Instruments, UAF42-Universal Active Filter datasheet. *http://www.ti.com/lit/ds/symlink/uaf42.pdf.*
[33] Pereira D.P., Girão P.S., Postolache O. (2001). Fitting Transducer Characteristics to Measured Data. IEEE Instrumentation & Measurement Magazine, 4(4), 26-39.
[34] National Instruments, LabVIEW 9.0. *http://www.ni.com/labview* .
[35] Cherry, Speed & Proximity Sensors, Geartooth Speed and Direction Sensor, part # SD100203 (2010 Sept.). *http://www.cherrycorp.com.*
[36] Analog Devices (2010). Accelerometer Design and Applications. Application Note AN-1057. *http://www.analog.com.*
[37] Kuorilehto M., et al. (2007). *Ultra-Low Energy Wireless Sensor Networks in Practice: theory, realization and deployment*. Finland: John Wiley and Sons, Ltd..
[38] Pereira J.M., Postolache O., Girão P.S. (2007). A Digitally Programmable A/D Converter for Smart Sensors Applications. *IEEE Transactions on Instrumentation and Measurement*, Vol.56, No.1, 158-163.
[39] IIT Kharagpur (2010), Introduction to Belt Drives, module 13, version 2 ME (2010 Sept.) *http://www.nptel.iitm.ac.in/courses.*
[40] Taylor C.F. (1985). *The Internal Combustion Engine in Theory and Practice*, Vol. 1 & 2, 2nd Edition. MIT Press.
[41] Danfoss, Variable speed driver, VLT 2800 Series (Sept. 2010). http://www.ledcontrols.co.uk.
[42] Lagarias J.C., Reeds J.A., Wright M.H., Wright P.E. (1998). Convergence Properties of the Nelder-Mead Simplex Method in Low Dimensions. *SIAM Journal of Optimization*, Vol. 9, No. 1, 112-147.
[43] Dias Pereira J.M., Serra A. Cruz, Girão P. (2000). Flexible ADC: a Dither and Oversampling Based Solution to Improve the Performance of ADC Systems. In *Proceedings of IMEKO World Congress 2000*. Wien, Austria, 103-108.